Transport spin polarization of noncollinear antiferromagnetic antiperovskites

Gautam Gurung, Ding-Fu Shao, and Evgeny Y. Tsymbal

Phys. Rev. Materials **5**, 124411 — Published 17 December 2021

DOI: 10.1103/PhysRevMaterials.5.124411

Transport Spin Polarization of Noncollinear Antiferromagnetic Antiperovskites

Gautam Gurung, Ding-Fu Shao,* and Evgeny Y. Tsymbal†

Department of Physics and Astronomy & Nebraska Center for Materials and Nanoscience, University of Nebraska, Lincoln, Nebraska 68588-0299, USA

Spin-polarized currents play a key role in spintronics. Recently, it has been found that antiferromagnets with a non-spin-degenerate band structure can efficiently spin-polarize electric currents, even though their net magnetization is zero. Among the antiferromagnetic metals with magnetic space group symmetry supporting this functionality, the noncollinear antiferromagnetic antiperovskites ANMn$_3$ (A = Ga, Ni, Sn, and Pt) are especially promising. This is due to their high Néel temperatures and a good lattice match to perovskite oxide substrates, offering possibilities of high structural quality heterostructures based on these materials. Here, we investigate the spin polarization of antiferromagnetic ANMn$_3$ metals using first-principles density functional theory calculations. We find that the spin polarization of the longitudinal currents in these materials is comparable to that in widely used ferromagnetic metals, and thus can be exploited in magnetic tunnel junctions and spin transfer torque devices. Moreover, for certain film growth directions, the out-of-plane transverse spin currents with a giant charge-to-spin conversion efficiency can be achieved, implying that the ANMn$_3$ antiperovskites can be used as efficient spin sources. These properties make ANMn$_3$ compounds promising for application in spintronics.

Spintronics exploits the spin degree of freedom in electronic devices for information processing and storage [1]. The magnetic order parameter is used as the state variable in these devices, and its detection and manipulation manifest the read and write operations of the stored information. Currents with sizable spin polarization play a central role in the electric performance of such operations used in realistic nanoscale spintronic devices. For example, in magnetic tunnel junctions (MTJs), which are employed in commercial magnetic random-access memories (MRAMs) [2], the electrical detection is realized via the tunneling magnetoresistance (TMR) effect signifying a response of the longitudinal spin-polarized charge current to the relative magnetization orientation of the two ferromagnetic electrodes [3-5]. On the other hand, the electric manipulation of magnetization can be achieved via a spin transfer torque driven by a longitudinal spin-polarized charge current [6,7] or via a spin Hall effect [8-10] where a transverse pure spin current is generated by spin-orbit coupling.

Ferromagnetic metals have been widely used in spintronics due to their finite magnetization which can easily spin-polarize electric currents. More recently, it was argued that antiferromagnetic spintronics is more promising, due to antiferromagnets being robust against magnetic perturbations, producing no stray fields, and exhibiting ultrafast spin dynamics [11 - 13]. Nevertheless, until recently antiferromagnets have been rarely considered efficient to generate spin-polarized currents. This is because most antiferromagnets exhibit a combined $\hat{T}\hat{O}$ symmetry, where $\hat{T}$ is the time reversal symmetry and $\hat{O}$ is a crystal symmetry. The $\hat{T}\hat{O}$ symmetry enforces Kramers' spin degeneracy and hence vanishing magnetization. While the antiferromagnetic order may lower the symmetry to support some unconventional spin Hall current useful for spin-orbit torque devices [14], the efficiency of the intrinsic charge-to-spin conversion of antiferromagnets [14-16] do not show obvious advantages compared to those of the widely used nonmagnetic heavy metal spin sources [15-17].

Recently, it was found that the $\hat{T}\hat{O}$ symmetry in antiferromagnets can be broken by the noncollinear magnetic order [18] or non-centrosymmetric arrangement of nonmagnetic atoms [19]. The broken $\hat{T}\hat{O}$ symmetry was shown to result in interesting electronic, magnetic and transport properties that previously were only known for ferromagnets, such as the anomalous Hall effect [18-34], the non-relativistic Zeeman-like band splitting [35-37], and the unconventional charge-to-spin conversion [38 - 43]. The emergence of electric currents with sizable spin polarization is particularly exciting, due to the possible use of these currents and the antiferromagnets generating them in spintronic devices [44-46].

Among the antiferromagnetic material candidates exhibiting the required magnetic space group symmetry to produce spin-polarized currents, Mn-based antiperovskite nitrides ANMn$_3$ (A = Ga, Ni, Sn, and Pt) [47] have a few advantages. In particular, these antiferromagnetic metals have sufficiently high Néel temperatures, often about room temperature [47,48]. Also their crystal structures match well to those of the widely used perovskite oxides, which allows the realization of high-quality epitaxial heterostructures for device fabrication [14,49].

In this work, based on first-principles density functional theory calculations, we explore the spin polarization of ANMn$_3$ (A = Ga, Ni, Sn, and Pt) antiferromagnetic metals [50]. We find that the longitudinal charge currents passing

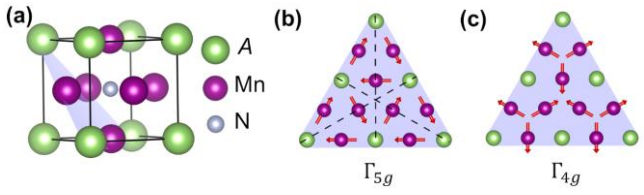

FIG. 1. (a) Atomic structure of antiperovskite ANMn$_3$. **(b, c)** The noncollinear alignment of Mn moments in the (111) plane for the antiferromagnteic Γ_{5g} (b) and Γ_{4g} (c) phases. Red arrows denote magnetic moments and dashed black lines indicate mirror planes $\widehat{M}_{0\bar{1}1}$, $\widehat{M}_{10\bar{1}}$, and $\widehat{M}_{\bar{1}10}$ for the Γ_{5g} phase.

Table 1. $\hat{T}$-odd spin conductivity tensors for the Γ_{5g} and Γ_{4g} phases of *A*NMn$_3$. The *x*, *y*, and *z* axes are set along the [100], [010] and [001] directions for a (001)-stacked film and along the $[\bar{1}10]$, [001], and [110] directions for a (110)-stacked film. The matrix elements in the parentheses only appear in the presence of spin-orbit coupling.

		$\boldsymbol{\sigma^x} = \begin{bmatrix} \sigma_{xx}^x & \sigma_{xy}^x & \sigma_{xz}^x \\ \sigma_{yx}^x & \sigma_{yy}^x & \sigma_{yz}^x \\ \sigma_{zx}^x & \sigma_{zy}^x & \sigma_{zz}^x \end{bmatrix}$	$\boldsymbol{\sigma^y} = \begin{bmatrix} \sigma_{xx}^y & \sigma_{xy}^y & \sigma_{xz}^y \\ \sigma_{yx}^y & \sigma_{yy}^y & \sigma_{yz}^y \\ \sigma_{zx}^y & \sigma_{zy}^y & \sigma_{zz}^y \end{bmatrix}$	$\boldsymbol{\sigma^z} = \begin{bmatrix} \sigma_{xx}^z & \sigma_{xy}^z & \sigma_{xz}^z \\ \sigma_{yx}^z & \sigma_{yy}^z & \sigma_{yz}^z \\ \sigma_{zx}^z & \sigma_{zy}^z & \sigma_{zz}^z \end{bmatrix}$
ANMn$_3$ (001)	$\boldsymbol{\Gamma_{5g}}$	$\begin{bmatrix} 0 & (-a) & (a) \\ (b) & -c & (-d) \\ (-b) & (d) & c \end{bmatrix}$	$\begin{bmatrix} c & (-b) & (d) \\ (a) & 0 & (-a) \\ (-d) & (b) & -c \end{bmatrix}$	$\begin{bmatrix} -c & (-d) & (b) \\ (d) & c & (-b) \\ (-a) & (a) & 0 \end{bmatrix}$
	$\boldsymbol{\Gamma_{4g}}$	$\begin{bmatrix} E & (A) & (A) \\ (B) & C & (D) \\ (B) & (D) & C \end{bmatrix}$	$\begin{bmatrix} C & (B) & (D) \\ (A) & E & (A) \\ (D) & (B) & C \end{bmatrix}$	$\begin{bmatrix} C & (D) & (B) \\ (D) & C & (B) \\ (A) & (A) & E \end{bmatrix}$
ANMn$_3$ (110)	$\boldsymbol{\Gamma_{5g}}$	$\begin{bmatrix} \frac{-a+b+c}{\sqrt{2}} & 0 & 0 \\ 0 & -\sqrt{2}c & (b-d) \\ 0 & (-a+d) & \frac{a-b+c}{\sqrt{2}} \end{bmatrix}$	$\begin{bmatrix} 0 & (-\sqrt{2}b) & c+d \\ (\sqrt{2}a) & 0 & 0 \\ c-d & 0 & 0 \end{bmatrix}$	$\begin{bmatrix} 0 & (-a-d) & \frac{a+b-c}{\sqrt{2}} \\ (b+d) & 0 & 0 \\ \frac{-a+b+c}{\sqrt{2}} & 0 & 0 \end{bmatrix}$
	$\boldsymbol{\Gamma_{4g}}$	$\begin{bmatrix} 0 & (A-D) & \frac{A-B-C+E}{\sqrt{2}} \\ (B-D) & 0 & 0 \\ \frac{-A+B-C+E}{\sqrt{2}} & 0 & 0 \end{bmatrix}$	$\begin{bmatrix} C-D & 0 & 0 \\ 0 & E & (\sqrt{2}\,A) \\ 0 & (\sqrt{2}\,B) & C+D \end{bmatrix}$	$\begin{bmatrix} \frac{-A-B+C+E}{\sqrt{2}} & 0 & 0 \\ 0 & \sqrt{2}C & (B+D) \\ 0 & (A+D) & \frac{A+B+C+E}{\sqrt{2}} \end{bmatrix}$

through *A*NMn$_3$ can have a sizable spin polarization, which allows using antiperovskites in magnetic tunnel junctions and spin transfer torque devices. Moreover, we show that the out-of-plane transverse spin currents with giant charge-to-spin conversion efficiencies can be achieved by controlling the film growth direction. These properties make *A*NMn$_3$ compounds promising for application in spintronics.

Figure 1(a) shows the crystal structure of the antiperovskite *A*NMn$_3$, which is similar to that of a perovskite except the cation and the anion having swapped positions (Fig. 1(a)). This structure hosts a frustrated Kagomé lattice in the (111) plane that favors noncollinear alignment of the antiferromagnetically coupled magnetic moments [47]. The antiperovskites exhibit interesting properties, such as magnetovolume [66], barocaloric [67], piezomagnetic [62, 63, 68], magnetoelectric [64, 69], anomalous Hall [24 - 29], and unconventional spin Hall [14] effects. One of the most common noncollinear antiferromagnetic orders in *A*NMn$_3$ is Γ_{5g} (typical for GaNMn$_3$), where the Mn magnetic moments form a chiral configuration with the 120° angle between each other within the (111) plane (Fig. 1(b)) [47, 61]. Γ_{5g} is a compensated antiferromagnetic phase due to three mirror planes $\widehat{M}_{0\bar{1}1}$, $\widehat{M}_{10\bar{1}}$, or $\widehat{M}_{\bar{1}10}$ perpendicular to the (111) plane in the magnetic space group $R\bar{3}m$ which prohibit the net magnetization. Another common noncollinear antiferromagnetic phase is Γ_{4g}, which can be obtained from the Γ_{5g} phase by rotating all magnetic moments about the [111] axis by 90° (Fig. 1(c)) [47]. The mirror symmetries are broken in the Γ_{4g} phase so that the corresponding magnetic space group $R\bar{3}m'$ allows an uncompensated magnetization (though very small) and the anomalous Hall effect [24,70].

We find that the magnetic group symmetries of both Γ_{5g} and Γ_{4g} phases support sizable longitudinal and transverse spin currents. In the diffusive transport regime, the spin conductivity has two contributions: [8,38]

$$\sigma_{ij}^k = -\frac{e\hbar}{\pi}\int \frac{d^3\vec{k}}{(2\pi)^3}\sum_{n,m}\frac{\Gamma^2 \mathrm{Re}\left(\langle n\vec{k}|J_i^k|m\vec{k}\rangle\langle m\vec{k}|v_j|n\vec{k}\rangle\right)}{\left[\left(E_F - E_{n\vec{k}}\right)^2 + \Gamma^2\right]\left[\left(E_F - E_{m\vec{k}}\right)^2 + \Gamma^2\right]}, \quad (1)$$

and

$$\sigma_{ij}^k = -\frac{2e}{\hbar}\int \frac{d^3\vec{k}}{(2\pi)^3}\sum_{m\neq n}\frac{\mathrm{Im}\left(\langle n\vec{k}|J_i^k|m\vec{k}\rangle\langle m\vec{k}|v_j|n\vec{k}\rangle\right)}{\left(E_{n\vec{k}} - E_{m\vec{k}}\right)^2}. \quad (2)$$

Here $J_i^k = \frac{1}{2}\{v_i, s_k\}$ is the spin current operator, Γ is the scattering rate in a constant relaxation time approximation, $f_{n\vec{k}}$ is the Fermi-Dirac distribution function for band *n* and wave vector $\vec{k}$, v_i and s_k are velocity and spin operators, respectively, and i, j and k are the spin-current, charge-current, and spin polarization directions, respectively. The spin conductivity σ_{ij}^k given by Eq. (1) is the Fermi surface property odd under time reversal symmetry ($\hat{T}$-odd). As a result, this contribution is allowed only for ferromagnetic and some antiferromagnetic metals without $\hat{T}$ or $\hat{T}\hat{O}$ symmetries, such as noncollinear antiferromagnetic *A*NMn$_3$. In these materials, the Fermi surface is intrinsically spin textured resulting in spin-polarized currents even in the absence of spin-orbit coupling. This leads to finite non-relativistic components of the $\hat{T}$-odd spin conductivity tensor. Spin-orbit coupling alters the spin texture and hence the spin conductivity tensor. However, due to the electronic structure of *A*NMn$_3$ at the Fermi energy (E_F) being majorly controlled by the Mn atoms which do not produce strong spin-orbit

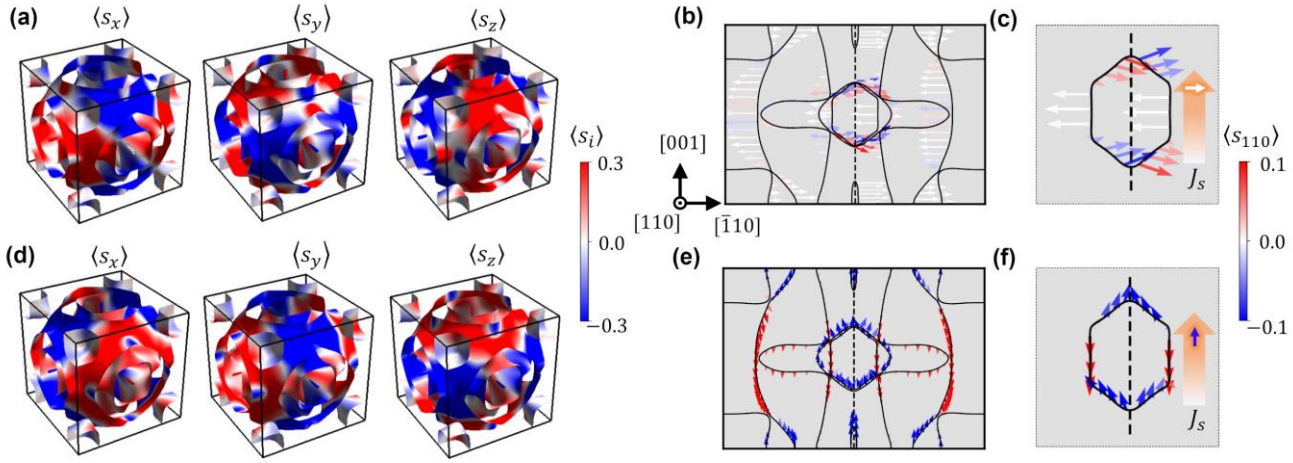

FIG. 2. (a) The spin-projected Fermi surface of $GaNMn_3$ in the Γ_{5g} phase. **(b)** The (110) plane cut of the Fermi surfaces shown in (a), where the solid lines denote the Fermi surface, the colored arrows denote the spin textures, and the dashed line denote the $M_{\bar{1}10}$ mirror plane. **(c)** The zoomed plot of (b) showing only the central Fermi pocket. **(d,e,f)** The same in (a,b,c) for $GaNMn_3$ in the Γ_{4g} phase.

coupling, these changes are not expected to be significant. (Note though that the spin-orbit coupling makes some σ_{ij}^k components finite, which were zero in its absence).

In contrast to the $\hat{T}$-odd σ_{ij}^k , the spin conductivity tensor given by Eq. (2) is determined by the interband contributions that are even under time reversal symmetry ($\hat{T}$-even). As a result, non-vanishing $\hat{T}$ -even σ_{ij}^k components can only appear in the presence of spin-orbit coupling. Therefore, these relativistic components are expected to be small compared to the non-relativistic components of the $\hat{T}$-odd σ_{ij}^k (see Supplemental Material [50]). Thus, in the following, we focus only on the $\hat{T}$-odd spin conductivity of $ANMn_3$.

Table I displays the $\hat{T}$-odd σ_{ij}^k of $ANMn_3$ according to the magnetic space group symmetry of the crystal. For a (001)-stacked $ANMn_3$ with the *x*, *y*, and *z* axes aligned along the [100], [010], and [001] crystal directions, there are four independent tensor components (denoted by *a*, *b*, *c*, and *d*) in the Γ_{5g} phase. These include the off-diagonal tensor components σ_{ij}^k $(i \neq j)$ which determine the transverse spin current generated by a longitudinal charge current and are related to the magnetic spin Hall effect proposed recently [38-41]. However, these off-diagonal components are relativistic in nature and are non-zero only in the presence of spin-orbit coupling. Therefore, these relativistic contributions to spin conductivity are not expected to be large, due the weak spin-orbit coupling in $ANMn_3$.

There are also non-relativistic diagonal components of the spin conductivity tensor σ_{jj}^k $(k \neq j)$. These components determine a longitudinal spin current carrying a transverse spin polarization generated by a longitudinal charge current. These diagonal components are non-zero even in the absence of spin-orbit coupling and hence are expected to be large. This implies that a longitudinal spin-polarized charge current can be produced in the compensated antiferromagnetic Γ_{5g} phase.

In order to obtain a more intuitive understanding of why the longitudinal charge current is spin-polarized, we use $GaNMn_3$ as a representative example and explore its momentum-dependent spin texture. Due to the broken $\hat{T}$ symmetry in antiferromagnetic $GaNMn_3$, the spin degeneracy is lifted and hence the spin expectation values $\langle s \rangle$ are finite. Since the $\hat{T}$-odd spin conductivity is a purely Fermi surface property (see Eq. (1)), it is the spin texture at the Fermi surface that matters. Figure 2(a) shows the calculated expectation values of the *x*, *y*, and *z* components of the spin at the Fermi surface of $GaNMn_3$ in the Γ_{5g} phase, indicating a rather intricate distribution. The same spin texture, but within the (110) plane, is displayed in Figure 2(b) and enlarged in Figure 2(c) to focus on the Fermi pocket at the center of the Brillouin zone. These spin textures can make the electric currents flowing along certain crystallographic directions of $GaNMn_3$ spin-polarized.

To demonstrate this, we consider symmetry transformations of the spin texture within this Fermi pocket. The inversion-symmetric fragments of the Fermi pocket have the same spin expectation values, since the inversion symmetry $\hat{P}$ does not change the spin:

$$\hat{P}(k_{110}, k_{\bar{1}10}, k_{001}) = (-k_{110}, -k_{\bar{1}10}, -k_{001}),$$
$$\hat{P}(\langle s_{110} \rangle, \langle s_{\bar{1}10} \rangle, \langle s_{001} \rangle) = (\langle s_{110} \rangle, \langle s_{\bar{1}10} \rangle, \langle s_{001} \rangle). \quad (3)$$

Further, the spin expectation values for the wave vectors being symmetric with respect to the $\widehat{M}_{\bar{1}10}$ mirror plane have the same $\langle s_{\bar{1}10} \rangle$ components but opposite $\langle s_{001} \rangle$ and $\langle s_{110} \rangle$ components. This is due to the mirror symmetry operation conserving the spin component normal to the mirror plane but flipping the spin component parallel to it:

$$\widehat{M}_{\bar{1}10}(k_{110}, k_{\bar{1}10}, k_{001}) = (k_{110}, -k_{\bar{1}10}, k_{001}),$$
$$\widehat{M}_{\bar{1}10}(\langle s_{110} \rangle, \langle s_{\bar{1}10} \rangle, \langle s_{001} \rangle) = (-\langle s_{110} \rangle, \langle s_{\bar{1}10} \rangle, -\langle s_{001} \rangle). \quad (4)$$

Table 2. Charge-to-spin conversion efficiency $\Phi(\sigma_{ij}^{k}) = \frac{2e}{\hbar}\sigma_{ij}^{k}/\sigma_{jj}$ (in %) in antiperovskite *A*NMn$_3$ (*A* = Ga, Ni, Sn, Pt) in Γ_{5g} and Γ_{4g} phases for (001)- and (110)-stacked films. Calcuationas are preformed in the presence of spin-orbit coupling for $\Gamma = 0.05$ eV. The *x*, *y*, and *z* are set along [100], [010] and [001] directions for (001)-stacked film and along $[\bar{1}10]$, [001], and [110] directions for a (110)-stacked film.

		$\boldsymbol{\Gamma_{5g}}$				$\boldsymbol{\Gamma_{4g}}$			
		GaNMn$_3$	NiNMn$_3$	SnNMn$_3$	PtNMn$_3$	GaNMn$_3$	NiNMn$_3$	SnNMn$_3$	PtNMn$_3$
*A*NMn$_3$ (001)	$\boldsymbol{\Phi(\sigma_{zz}^{x})}$	-20.7	13.3	-27.0	14.2	-12.3	7.7	-16.0	10.2
	$\boldsymbol{\Phi(\sigma_{zz}^{z})}$	0.0	0.0	0.0	0.0	24.4	-15.1	31.2	-18.1
	$\boldsymbol{\Phi(\sigma_{zx}^{x})}$	-0.4	-0.7	-0.7	-3.4	-0.1	-0.3	0.6	-1.8
	$\boldsymbol{\Phi(\sigma_{zx}^{y})}$	-0.3	-0.4	-0.6	-0.01	-0.8	-0.3	-0.4	-3.8
	$\boldsymbol{\Phi(\sigma_{zx}^{z})}$	0.1	0.5	-0.1	1.0	-0.3	-0.2	0.3	-0.1
*A*NMn$_3$ (110)	$\boldsymbol{\Phi(\sigma_{zz}^{x})}$	-15.0	8.6	-19.5	6.9	0.0	0.0	0.0	0.0
	$\boldsymbol{\Phi(\sigma_{zz}^{z})}$	0.0	0.0	0.0	0.0	8.3	-5.6	11.4	-6.9
	$\boldsymbol{\Phi(\sigma_{zx}^{x})}$	0.0	0.0	0.0	0.0	26.1	-16.2	33.6	-21.2
	$\boldsymbol{\Phi(\sigma_{zx}^{y})}$	-21.0	12.9	-27.6	14.2	0.0	0.0	0.0	0.0
	$\boldsymbol{\Phi(\sigma_{zx}^{z})}$	14.4	-9.5	18.5	-11.7	0.0	0.0	0.0	0.0

As a result, the longitudinal electric current parallel to the $(\bar{1}10)$ plane, such as the current along the [001] direction shown in Fig. 2(c) is polarized by this spin texture. The associated spin current J_c has a finite $\langle s_{\bar{1}10}\rangle$ component but zero $\langle s_{110}\rangle$ and $\langle s_{001}\rangle$ components, since only $\langle s_{\bar{1}10}\rangle$ is even with respect to $\widehat{M}_{\bar{1}10}$. This implies finite matrix elements of the longitudinal spin conductivity tensor $\sigma_{zz}^{x} = -\sigma_{zz}^{y} = c$, as shown in Table I for *A*NMn$_3$ in the Γ_{5g} phase.

In contrast to the Γ_{5g} phase, the Γ_{4g} phase of *A*NMn$_3$ has five independent components (denoted by *A*, *B*, *C*, *D*, and *E*) of the $\hat{T}$-odd spin conductivity tensor for a (001)-stacked *A*NMn$_3$. We find that both the diagonal components with spin polarization normal to the charge current direction, $\sigma_{jj}^{k} = C$ $(k \neq j)$, and those parallel to it, $\sigma_{jj}^{j} = E$, do not vanish in the absence of spin-orbit coupling. This can be illustratively understood by analyzing the spin projected Fermi surfaces of the Γ_{4g} GaNMn$_3$ (Fig. 2(d-f)). The spin textures in the Γ_{4g} phase are very different from those in the Γ_{5g} phase due to different magnetic-space group symmetry. The mirror $\widehat{M}_{\bar{1}10}$ plane is broken in the Γ_{4g} phase, while a combined $\hat{T}\widehat{M}_{\bar{1}10}$ symmetry is preserved, which transforms the wave vector and the spin as follows:

$$\hat{T}\widehat{M}_{\bar{1}10}(k_{110}, k_{\bar{1}10}, k_{001}) = (-k_{110}, k_{\bar{1}10}, -k_{001}),$$
$$\hat{T}\widehat{M}_{\bar{1}10}(\langle s_{110}\rangle, \langle s_{\bar{1}10}\rangle, \langle s_{001}\rangle) = (\langle s_{110}\rangle, -\langle s_{\bar{1}10}\rangle, \langle s_{001}\rangle). \quad (5)$$

This symmetry together with inversion symmetry $\hat{P}$ (Eq. (3)) implies that $\langle s_{\bar{1}10}\rangle$ is antisymmetric and $\langle s_{110}\rangle$ and $\langle s_{001}\rangle$ are symmetric with respect to $(\bar{1}10)$ plane. Therefore, a longitudinal electric current parallel to the $(\bar{1}10)$ plane, such as that along the [001] direction, becomes spin-polarized with finite $\langle s_{110}\rangle$ and $\langle s_{001}\rangle$ components and a zero $\langle s_{\bar{1}10}\rangle$ component. This implies finite longitudinal spin conductivities $\sigma_{zz}^{x} = \sigma_{zz}^{y} = C$ and $\sigma_{zz}^{x} = \sigma_{zz}^{z} = E$ as shown in Table I.

The efficiency of the $\hat{T}$-odd spin current generation can be estimated by calculating a percentage spin conductivity ratio $\Phi(\sigma_{ij}^{k}) = \frac{2e}{\hbar}\sigma_{ij}^{k}/\sigma_{jj}$. Here σ_{jj} is a conductivity of the longitudinal charge current J_c used to generate the spin current J_s with conductivity σ_{ij}^{k}, which can be calculated by replacing the spin current operator J_i^k in Eq. (1) by the charge current operator $J_i = -ev_i$. $\Phi(\sigma_{zj}^{k})$ serves as a figure of merit for the performance of realistic spintronic devices. In particular, $\Phi(\sigma_{zx}^{k})$ represents the spin Hall angle in spin-torque devices with current-in-plane (CIP) geometry, where an out-of-plane spin current is generated by an in-plane charge current. Similarly, $\Phi(\sigma_{zz}^{k})$ measures the degree of spin polarization for an out-of-plane charge current in devices with current-perpendicular-to-plane (CPP) geometry, such as MTJs.

We calculate $\Phi(\sigma_{zj}^{k})$ for *A*NMn$_3$ (*A* = Ga, Ni, Sn, Pt) compounds assuming they are stacked in the (001) plane. Table 2 shows the calculated results for $\Gamma = 0.05$ eV which provides realistic conductivity σ_{zz} of the compounds. For the longitudinal spin conductivity, we find that $\Phi(\sigma_{zz}^{i})$ is sizable for all *A*NMn$_3$ antiferromagnets we investigated. Especially, we obtain $\Phi(\sigma_{zz}^{x}) = -20.7\%$ for GaNMn$_3$ which exhibits a Γ_{5g} ground state, and $\Phi(\sigma_{zz}^{x}) = -16.0\,\%$ and $\Phi(\sigma_{zz}^{z}) = 31.2\%$ for SnNMn$_3$ which has a high-temperature Γ_{4g} state. These sizable spin polarizations of the longitudinal current in antiferromagnetic antiperovskites are comparable to those in ferromagnetic metals, such as Fe, Co, and Ni [71-73], indicating their potential for spintronic applications, such as

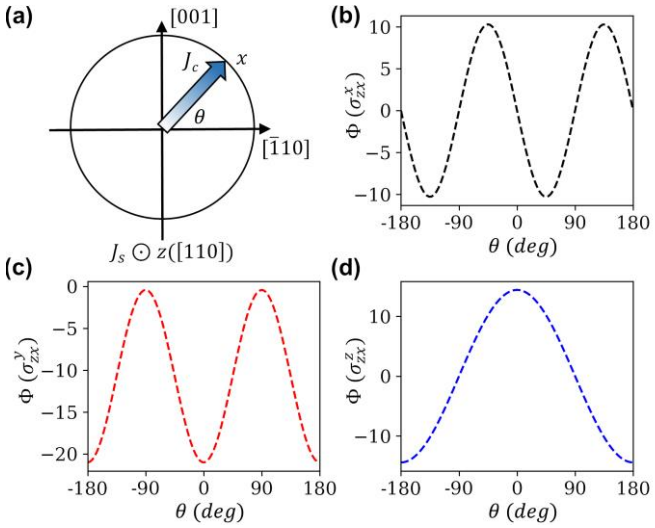

FIG. 3. (a) The schematic of charge-to-spin conversion in an *A*NMn$_3$ (110) film. An out-of-plane spin current J_s along the [110] (z) direction is generated by applying an in-plane longitudinal charge current J_c along x direction which is away from [$\bar{1}$10] direction by the angle θ. **(b, c, d)** Charge-to-spin conversion efficiency $\Phi(\sigma_{zx}^k)$as a function of the longitudinal charge current direction for GaNMn$_3$ (110)-stacked films in the Γ_{5g} phase.

antiferromagnetic tunnel junctions discussed below. We note that our results are robust with respect to disorder scattering, as follows from our calculations of $\Phi(\sigma_{zz}^k)$ as a function of Γ shown in Supplementary Figure S1 [50].

On the contrary, the transverse spin conductivity ratio $\Phi(\sigma_{zx}^k)$ is negligible for *A*NMn$_3$ (001) (Table 2). This is understandable since the non-relativistic spin texture does not contribute to σ_{zx}^k and the effect appears entirely due to small spin-orbit coupling. However, although *A*NMn$_3$ is not efficient for generating transverse spin currents in (001)-stacked films, it can form a good spin current source for spin-torque devices by engineering the *A*NMn$_3$ growth direction. The related spin conductivity tensors for a film with different orientation can be obtained by applying transformation

$$\sigma_{i'j'}^{k'} = \sum_{k,i,j} R_{k'k} R_{i'i} R_{j'j} \sigma_{ij}^k , \qquad (S1)$$

where σ_{ij}^k is the spin conductivity for a (001)-stacked film with coordinate system (x, y, z), $\sigma_{i'j'}^{k'}$ is the spin conductivity of a film with coordinate system (x', y', z'), R is the rotation matrix to transform the coordinate system (x, y, z) to (x', y', z'). A non-relativistic spin texture contribution to $\Phi(\sigma_{zx}^k)$ may be allowed by the magnetic-space group symmetry after the rotation transformation.

As an example, Table 1 shows the spin conductivity tensor for *A*NMn$_3$ (110) in the Γ_{5g} and Γ_{4g} phases. It is seen that when the charge current direction (x) is along the [$\bar{1}$10] direction, finite σ_{zx}^y and σ_{zx}^z appear in the Γ_{5g} phase, and a finite σ_{zx}^x appear in the Γ_{4g} phase, even in the absence of spin-orbit coupling. Table 2 shows calculated $\Phi(\sigma_{zx}^k)$ for *A*NMn$_3$ (*A* = Ga, Ni, Sn, and Pt) (110) films. For the Γ_{5g} ground state in GaNMn$_3$, we find large $\Phi(\sigma_{zx}^y) = -21.0\%$ and $\Phi(\sigma_{zx}^z) = 14.4\%$, which are comparable or even larger than these for the reported spin Hall angle in widely used spin source materials such as Pt [74-76].

Moreover, the transverse σ_{zx}^x component in the Γ_{5g} phase can be engineered by tilting the in-plane longitudinal current direction x from [110] by an angle θ (Fig. 3(a)). In this case, the σ_{zx}^k components are functions of θ as follows:

$$\sigma_{zx}^x = \frac{-a+c}{2}\sin 2\theta ,$$
$$\sigma_{zx}^y = \frac{1}{2}(a+c-2d) - \frac{1}{2}(a-c)\cos 2\theta ,$$
$$\sigma_{zx}^z = -\frac{a+b+c}{\sqrt{2}}\cos\theta . \qquad (6)$$

Figures 3(b-d) show the respective variations of σ_{zx}^k as functions of θ for GaNMn$_3$ (110). Similar angular dependences of σ_{zx}^k for the ground states of NiNMn$_3$, SnNMn$_3$, and PtNMn$_3$ (110) films can be found in Supplemental Material [50].

The predicted efficient generation of the longitudinal and transverse currents with sizable spin polarization allows promising spintronic devices based on noncollinear antiferromagnetic *A*NMn$_3$. Here we propose two types of spintronic devices, as shown in Figure 4. The first one is an antiferromagnetic tunnel junction [38], where the two *A*NMn$_3$ electrodes are separated by an insulating nonmagnetic layer [Fig. 4(a)]. The CPP longitudinal spin polarized current is controlled by the relative orientation of the magnetic order parameters in the *A*NMn$_3$ reference and free layers. Due to a large spin polarization of the longitudinal current, the TMR effect is expected to be sizable and hence can be used to efficiently detect the magnetic order parameter in *A*NMn$_3$. The spin polarized current can be also used to generate the spin-transfer torque for switching *A*NMn$_3$ [70, 77-79].

The second spintronic device is a CIP spin-torque device, where an ANMn$_3$ (110) layer is used as a spin source to generate an out-of-plane spin current which enters the top ferromagnetic layer and exerts a torque on its magnetization

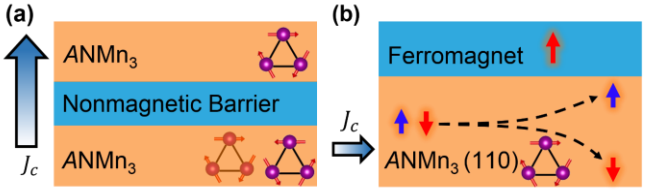

FIG. 4. (a) The schematic of an antiferromagnetic tunnel junction using *A*NMn$_3$ as the electrodes, where the transport of the out-of-plane longitudinal spin polarized current is controlled by the relative orientation of the magnetic moments between two *A*NMn$_3$ layers. **(b)** The schematic of a spin torque device with CIP geometry. An in-plane charge current passes through *A*NMn$_3$ (110) layer and generates an out-of-plane spin current carrying sizable spin polarization collinear to the spin current direction. This spin current can exert a torque on the perpendicular magnetization in the top ferromagnetic layer for an efficient switching.

(Fig. 4(b)). Since ANMn$_3$ (110) layer exhibits large $\Phi(\sigma_{zx}^{z})$, the spin current can carry sizable spin component collinear to the spin current direction, which is necessary for switching a ferromagnet with perpendicular anisotropy required for high-density spintronic devices.

We note that the symmetries of bulk antiperovskites are lowered at the interfaces of such devices which may affect spin-dependent transport properties, such as the TMR and spin-transfer torque. It was found, however, that in realistic antiferromagnet/nonmagnet systems, these effects were not essential for the device performance [11, 80, 81]. We expect therefore that the predicted bulk properties would largely control functional properties of the device structures based on antiferromagnetic antiperovskites.

In conclusion, based on first-principles density functional theory calculations, we have predicted that the noncollinear antiferromagnetic antiperovskites ANMn$_3$ (A = Ga, Ni, Sn, and Pt) support electric currents with sizable spin polarization. We found that the calculated spin polarization of the longitudinal currents can be comparable to that in widely used ferromagnetic metals, which makes the antiperovskites promising for using in antiferromagnetic tunnel junction and spin transfer torque devices. Furthermore, we demonstrated that by controlling the film growth direction, the out-of-plane transverse spin currents with sizable charge-to-spin conversion efficiencies can be achieved, which implies that the ANMn$_3$ compounds can serve as effective spin source materials. These properties make noncollinear antiferromagnetic antiperovskites promising for realistic applications in spintronics.

Acknowledgements: This work was supported by the Office of Naval Research (ONR grant N00014-20-1-2844) and by the National Science Foundation (NSF) through EPSCoR RII Track-1 (NSF Award OIA-2044049) program. Computations were performed at the University of Nebraska Holland Computing Center. The figures were created using VESTA [82], FermiSurfer [83] and Matplotlib.

* dfshao@unl.edu
† tsymbal@unl.edu

[1] E. Y. Tsymbal and I. Žutić, Eds., *Spintronics Handbook: Spin Transport and Magnetism*, 2-nd edition (CRC press, 2019).
[2] A. V. Khvalkovskiy, D. Apalkov, S. Watts, R. Chepulskii, R. S. Beach, A. Ong, X. Tang, A. Driskill-Smith, W. H. Butler, P. B. Visscher, D. Lottis, E. Chen, V. Nikitin, and M. Krounbi, Basic principles of STT-MRAM cell operation in memory arrays. *J. Phys. D* **46**, 074001 (2013).
[3] M. Julliere, Tunneling between ferromagnetic films. *Phys. Lett.* **54A**, 225 (1975).
[4] J. S. Moodera, L. R. Kinder, T. M. Wong, and R. Meservey, Large magnetoresistance at room temperature in ferromagnetic thin film tunnel junctions. *Phys. Rev. Lett.* **74**, 3273 (1995).
[5] E. Y. Tsymbal, O. N. Mryasov, and P. R. LeClair, Spin-dependent tunneling in magnetic tunnel junctions. *J. Physics: Condensed Matter* **15**, R109-R142 (2003).
[6] J. C. Slonczewski, Conductance and exchange coupling of two ferromagnets separated by a tunneling barrier. *Phys. Rev. B* **39**, 6995 (1989).
[7] D. Ralph and M. Stiles, Spin transfer torques. *J. Magn.Magn. Mater*. **320**, 1190 (2008).
[8] J. Sinova, S. O. Valenzuela, J. Wunderlich, C. H. Back, and T. Jungwirth, Spin Hall effects, *Rev. Mod. Phys.* **87**, 1213 (2015).
[9] I. M. Miron, K. Garello, G. Gaudin, P.-J. Zermatten, M. V. Costache, S. Auffret, S. Bandiera, B. Rodmacq, A. Schuhl, and P. Gambardella. Perpendicular switching of a single ferromagnetic layer induced by in-plane current injection, *Nature* **476**, 189 (2011).
[10] L. Liu, C.-F. Pai, Y. Li, H.W. Tseng, D. C. Ralph, and R. A. Buhrman, Spin-torque switching with the giant spin Hall effect of tantalum. *Science* **336**, 555 (2012).
[11] V. Baltz, A. Manchon, M. Tsoi, T. Moriyama, T. Ono, and Y. Tserkovnyak, Antiferromagnetic spintronics. *Rev. Mod. Phys.* **90**, 015005 (2018).
[12] T. Jungwirth, X. Marti, P. Wadley, and J. Wunderlich, Antiferromagnetic spintronics. *Nat. Nanotechnol.* **11**, 231 (2016).
[13] T. Jungwirth, J. Sinova, A. Manchon, X. Marti, J. Wunderlich, and C. Felser, The multiple directions of antiferromagnetic spintronics. *Nat. Phys.* **14**, 200 (2018).

[14] T. Nan, C. X. Quintela, J. Irwin, G. Gurung, D. -F. Shao, J. Gibbons, N. Campbell, K. Song, S. Y. Choi, L. Guo, R. D. Johnson, P. Manuel, R. V. Chopdekar, I. Hallsteinsen, T. Tybell, P. J. Ryan, J. W. Kim, Y. S. Choi, P. G. Radaelli, D. C. Ralph, E. Y. Tsymba, M. S. Rzchowski, and C. B. Eom, Controlling spin current polarization through non-collinear antiferromagnetism. *Nat. Commun.* **11**, 4671 (2020).

[15] F. Freimuth, S. Blügel, and Y. Mokrousov, Anisotropic spin Hall effect from first principles. *Phys. Rev. Lett.* **105**, 246602 (2010).

[16] Y. Zhang, Y. Sun, H. Yang, J. Železný, S. P. P. Parkin, C. Felser, and B. Yan, Strong anisotropic anomalous Hall effect and spin Hall effect in the chiral antiferromagnetic compounds Mn_3X (X = Ge, Sn, Ga, Ir, Rh, and Pt). *Phys. Rev. B* **95**, 075128 (2017).

[17] G. Y. Guo, S. Murakami, T.-W. Chen, and N. Nagaosa, Intrinsic spin Hall effect in platinum: First-Principles Calculations. *Phys. Rev. Lett.* **100**, 096401 (2008).

[18] H. Chen, Q. Niu, and A. H. MacDonald, Anomalous Hall effect arising from noncollinear antiferromagnetism. *Phys. Rev. Lett*. **112**, 017205 (2014).

[19] L. Šmejkal, R. González-Hernández, T. Jungwirth, and J. Sinova, Crystal time-reversal symmetry breaking and spontaneous Hall effect in collinear antiferromagnets. *Sci. Adv.* **6**, eaaz8809 (2020).

[20] J. Kübler and C. Felser, Non-collinear antiferromagnets and the anomalous Hall effect. *EPL* **108**, 67001 (2014).

[21] S. Nakatsuji, N. Kiyohara, and T. Higo, Large anomalous Hall effect in a non-collinear antiferromagnet at room temperature. *Nature* **527**, 212 (2015).

[22] A. K. Nayak, J. E. Fischer, Y. Sun, B. Yan, J. Karel, A. C. Komarek, C. Shekhar, N. Kumar, W. Schnelle, J. Kübler, C. Felser, and S. P. P. Parkin, Large anomalous Hall effect driven by a nonvanishing Berry curvature in the noncollinear antiferromagnet Mn_3Ge. *Sci. Adv.* **2**, e1501870 (2016).

[23] Y. Zhang, Y. Sun, H. Yang, J. Železný, S. P. P. Parkin, C. Felser, and B. Yan, Strong anisotropic anomalous Hall effect and spin Hall effect in the chiral antiferromagnetic compounds Mn_3X (X = Ge, Sn, Ga, Ir, Rh, and Pt). *Phys. Rev. B* **95**, 075128 (2017).

[24] G. Gurung, D.-F. Shao, T. R. Paudel, and E. Y. Tsymbal, Anomalous Hall conductivity of non-collinear magnetic antiperovskites. *Phys. Rev. Mater.* **3**, 044409 (2019).

[25] D. Boldrin, I. Samathrakis, J. Zemen, A. Mihai, B. Zou, B. Esser, D. McComb, P. Petrov, H. Zhang, and L. F. Cohen, The anomalous Hall effect in non-collinear antiferromagnetic Mn3NiN thin films. *Phys. Rev. Mater.* **3**, 094409 (2019).

[26] X. Zhou, J.-P. Hanke, W. Feng, F. Li, G.-Y. Guo, Y. Yao, S. Blügel, and Y. Mokrousov, Spin-order dependent anomalous Hall effect and magneto-optical effect in the noncollinear antiferromagnets Mn_3XN with X = Ga, Zn, Ag, or Ni. *Phys. Rev. B* **99**, 104428 (2019).

[27] K. Zhao, T. Hajiri, H. Chen, R. Miki, H. Asano, and P. Gegenwart, Anomalous Hall effect in the noncollinear antiferromagnetic antiperovskite $Mn_3Ni_{1-x}Cu_xN$. *Phys. Rev. B* **100**, 045109 (2019).

[28] V. T. N. Huyen, M.-T. Suzuki, K. Yamauchi, and T. Oguchi, Topology analysis for anomalous Hall effect in the noncollinear antiferromagnetic states of Mn_3AN (A= Ni, Cu, Zn, Ga, Ge, Pd, In, Sn, Ir, Pt), *Phys. Rev. B* **100**, 094426 (2019).

[29] Y. You, H. Bai, X. Chen, Y. Zhou, X. Zhou, F. Pan, and C. Song, Room temperature anomalous Hall effect in antiferromagnetic Mn_3SnN films. *Appl. Phys. Lett*. **117**, 222404 (2020).

[30] X. Li, A. H. MacDonald, and H. Chen, Quantum anomalous Hall effect through canted antiferromagnetism. *arXiv*:1902.10650 (2019).

[31] N. J. Ghimire, A. S. Botana, J. S. Jiang, J. Zhang, Y.-S. Chen, and J. F. Mitchell, Large anomalous Hall effect in the chiral-lattice antiferromagnet $CoNb_3S_6$. *Nat. Commun.* **9**, 3280 (2018).

[32] D. -F. Shao, J. Ding, G. Gurung, S.-H. Zhang, and E. Y. Tsymbal, Interfacial crystal Hall effect reversible by ferroelectric polarization. *Phys. Rev. Applied* **15**, 024057 (2021).

[33] K. Samanta, M. Ležaić, M. Merte, F. Freimuth, S. Blügel, and Y. Mokrousov, Crystal Hall and crystal magneto-optical effect in thin films of $SrRuO_3$. *Journal of Applied Physics* **127**, 213904 (2020).

[34] J. Kipp, K. Samanta, F. R. Lux, M. Merte, D. Go, J.-P. Hanke, M. Redies, F. Freimuth, S. Blügel, M. Ležaić, and Y. Mokrousov, The chiral Hall effect in canted ferromagnets and antiferromagnets. *Communications Physics* **4**, 99 (2021).

[35] S. Hayami, Y. Yanagi, and H. Kusunose, Momentum-dependent spin splitting by collinear antiferromagnetic ordering. *J. Phys. Soc. Jpn.* **88**, 123702 (2019).

[36] L.-D. Yuan, Z. Wang, J. -W. Luo, E. I. Rashba, and A. Zunger, Giant momentum-dependent spin splitting in centrosymmetric low-Z antiferromagnets. *Phys. Rev. B* **102**, 014422 (2020).

[37] L.-D. Yuan, Z. Wang, J. -W. Luo, and A. Zunger, Prediction of low-Z collinear and noncollinear antiferromagnetic compounds having momentum-dependent spin splitting even without spin-orbit coupling. *Phys. Rev. Mater.* **5**, 014409 (2021).

[38] J. Železný, Y. Zhang, C. Felser, and B. Yan, Spin-polarized current in noncollinear antiferromagnets. *Phys. Rev. Lett.* **119**, 187204 (2017).

[39] M. Kimata, H. Chem, K. Kondou, S. Sugimoto, P. K. Muduli, M. Ikhlas, Y. Omori, T. Tomita, A. H. MacDonald, S. Nakatsuji, and Y. Otani, Magnetic and magnetic inverse spin Hall effects in a non-collinear antiferromagnet. *Nature* **565**, 627 (2019).

[40] A. Mook, R. R. Neumann, A. Johansson, J. Henk, and I. Mertig, Origin of the magnetic spin Hall effect: Spin current vorticity in the Fermi sea. *Phys. Rev. Research* **2**, 023065 (2020).

[41] R. González-Hernández, L. Šmejkal, K. Výborný, Y. Yahagi, J. Sinova, T. Jungwirth, J. Železný, Efficient electrical spin-splitter based on non-relativistic collinear antiferromagnetism. *Phys. Rev. Lett.* **126**, 127701 (2021).

[42] M. Naka, S. Hayami, H. Kusunose, Y. Yanagi, Y. Motome, and H. Seo, Spin current generation in organic antiferromagnets. *Nat. Commun.* **10**, 4305 (2019).

[43] H. Y. Ma, M. Hu, N. Li, J. Liu, W. Yao, J.-F. Jia, and J. Liu, Multifunctional antiferromagnetic materials with giant piezomagnetism and noncollinear spin current, *Nat. Commun.* **12**, 2846 (2021).

[44] D. -F. Shao, S. H. Zhang, M. Li, C. B. Eom and E. Y Tsymbal, Spin-neutral currents for spintronics. *Nat Commun* **12**, 7061 (2021).

[45] S. Hu, D. -F. Shao, H. Yang, M. Tang, Y. Yang, W. Fan, S. Zhou, E. Y. Tsymbal, and X. Qiu, Efficient field-free perpendicular magnetization switching by a magnetic spin Hall effect. *arXiv*:2103.09011 (2021).

[46] L. Šmejkal, A. B. Hellenes, R. G. Hernández, J. Sinova, and T. Jungwirth, Giant and tunneling magnetoresistance effects from anisotropic and valley-dependent spin-momentum interactions in antiferromagnets, *arXiv:*2103.12664 (2021).

[47] D. Fruchart and E. F. Bertaut, Magnetic studies of the metallic perovskite-type compounds of manganese. *J. Phys. Soc. Jap.* **44**, 781 (1978).

[48] K. Takenaka, M. Ichigo, T. Hamada, A. Ozawa, T. Shibayama, T. Inagaki, and K. Asano, Magnetovolume effects in manganese nitrides with antiperovskite structure, *Sci. Technol. Adv. Mater* **15**, 015009 (2014).

[49] C. X. Quintela, K. Song, D. -F. Shao, L. Xie, T. Nan, T. R. Paudel, N. Campbell, X. Pan, T. Tybell, M. S. Rzchowski, E. Y. Tsymbal, S. Y. Choi, and C. B. Eom, Epitaxial antiperovskite/perovskite heterostructures for materials design. *Sci. Adv.* **6**, eaba4017 (2020).

[50] See Supplemental Material [url] for the description of calculation methods, magnetic ground state of antiperovskites $ANMn_3$, $\hat{T}$- odd and even charge-to-spin conversion efficiency, which includes Refs. [51-65] .

[51] P. Giannozzi et al., Quantum ESPRESSO: A modular and open-source software project for quantum simulations of materials. *J. Phys.: Condens. Matt*. **21**, 395502 (2009).

[52] D. Vanderbilt, Soft self-consistent pseudopotentials in a generalized eigenvalue formalism. *Phys. Rev. B* **41**, 7892 (1990).

[53] J. P. Perdew, K. Burke, and M. Ernzerhof, Generalized gradient approximation made simple. *Phys. Rev. Lett.* **77**, 3865 (1996).

[54] J. Železný, *https://bitbucket.org/zeleznyj/wannier-linear-response/wiki/Home*.

[55] N. Marzari, A. A. Mostofi, J. R. Yates, I. Souza, and D. Vanderbilt, Maximally localized Wannier functions: Theory and applications. *Rev. Mod. Phys.* **84,** 1419 (2012).

[56] G. Pizzi, V. Vitale, R. Arita, S. Blügel, F. Freimuth, G. Géranton, M. Gibertini, D. Gresch, C. Johnson, T.Koretsune, J. Ibañez-Azpiroz, H. Lee, J. M. Lihm, D. Marchand, A. Marrazzo, Y. Mokrousov, J. I. Mustafa, Y. Nohara, Y. Nomura, L. Paulatto, S. Poncé, T. Ponweiser, J. Qiao, F. Thöle, S. S. Tsirkin, M. Wierzbowska, N. Marzari, D. Vanderbilt, I. Souza, A. A. Mostofi, and J. R. Yates, Wannier90 as a community code: New features and applications. *J. Phys. Cond. Mat.* **32**, 165902 (2020).

[57] J. Železný, *https://bitbucket.org/zeleznyj/linear*.

[58] K. Momma, and F. Izumi, VESTA: a three-dimensional visualization system for electronic and structural analysis. *J. Appl. Crystal.* **41**, 653 (2008).

[59] M. Kawamura, Fermisurfer: Fermi-surface viewer providing multiple representation schemes, *Comp. Phys. Commun.* **239**, 197 (2019).

[60] E. F. Bertaut, D. Fruchart, J. P. Bouchaud, and R. Fruchart, Diffraction neutronique de Mn_3GaN. *Solid St. Commun.* **6**, 251 (1968).

[61] K. Shi, Y. Sun, J. Yan, S. Deng, L. Wang, H. Wu, P. Hu, H. Lu, M. I. Malik, Q. Huang, and C. Wang, Baromagnetic effect in antiperovskite $Mn_3Ga_{0.95}N_{0.94}$ by neutron powder diffraction analysis. *Adv. Mater.* **28**, 3761 (2016).

[62] P. Lukashev, R. F. Sabirianov, and K. Belashchenko, Theory of piezomagnetic effect in Mn-based antiperovskites. *Phys. Rev. B* **78**, 184414 (2008).

[63] J. Zemen, Z. Gercsi, and K. G. Sandeman, Piezomagnetism as a counterpart of the magnetovolume effect in magnetically frustrated Mn-based antiperovskite nitrides. *Phys. Rev. B* **96**, 024451 (2017).

[64] D. -F. Shao, G. Gurung, T. R. Paudel, and E. Y. Tsymbal, Electrically reversible magnetization at the antiperovskite/ perovskite interface. *Phys. Rev. Materials* **3,** 024405 (2019).

[65] H. K. Singh, I. Samathrakis, N. M. Fortunato, J. Zemen, C. Shen, O. Gutfleisch, and H. Zhang, Multifunctional antiperovskites driven by strong magnetostructural coupling, *npj Comput. Mater.* **7**, 98 (2021).

[66] K. Takenaka, M. Ichigo, T. Hamada, A. Ozawa, T. Shibayama, T. Inagaki, and K. Asano, Magnetovolume effects in manganese nitrides with antiperovskite structure. *Sci. Tech. Adv. Mat.* **15**, 015009 (2014).

[67] D. Matsunami, A. Fujita, K. Takenaka, and M. Kano, Giant barocaloric effect enhanced by the frustration of the antiferromagnetic phase in Mn_3GaN. *Nat. Mater.* **14**, 73 (2015).

[68] D. Boldrin, A. P. Mihai, B. Zou, J. Zemen, R. Thompson, E. Ware, B. V. Neamtu, L. Ghivelder, B. Esser, D. W. McComb, P. Petrov, and L. F. Cohen, Giant piezomagnetism in Mn_3NiN. *ACS Appl. Mater. & Int.* **10**, 18863 (2018).

[69] P. Lukashev, K. D. Belashchenko, and R. F. Sabirianov, Large magnetoelectric effect in ferroelectric/piezomagnetic heterostructures. *Phys. Rev. B* **84**, 133420 (2011).

[70] G. Gurung, D. -F. Shao, and E. Y. Tsymbal, Spin-torque switching of noncollinear antiferromagnetic antiperovskites. *Phys. Rev. B* **101**, 140405(R) (2020).

[71] R. J. Soulen Jr., J. M. Byers, M. S. Osofsky, B. Nadgorny, T. Ambrose, S. F. Cheng, P. R. Broussard, C. T. Tanaka, J. Nowak, J. S. Moodera, A. Barry, and J. M. D. Coey, Measuring the spin polarization of a metal with a superconducting point contact. *Science* **282**, 85, (1998)

[72] S. K. Upadhyay, A. Palanisami, R. N. Louie, and R. A. Buhrman, Probing ferromagnets with Andreev reflection. *Phys. Rev. Lett.* **81**, 3247 (1998).

[73] I. I. Mazin, How to Define and Calculate the Degree of Spin Polarization in Ferromagnets. *Phys. Rev. Lett.* **83**, 1427 (1999).

[74] X. Tao, Q. Liu, B. Miao, R. Yu, Z. Feng, L. Sun, B. You, J. Du, K. Chen, S. Zhang, L. Zhang, Z. Yuan, D. Wu, and H. Ding, Self-consistent determination of spin Hall angle and spin diffusion length in Pt and Pd: The role of the interface spin loss. *Sci. Adv.* **4**, eaat1670 (2018).

[75] A. J. Berger, E. R. J. Edwards, H. T. Nembach, O. Karis, M. Weiler, and T. J. Silva, Determination of the spin Hall effect and the spin diffusion length of Pt from self-consistent fitting of damping enhancement and inverse spin-orbit torque measurements. *Phys. Rev. B* **98**, 024402 (2018).

[76] S. Keller, L. Mihalceanu, M. R. Schweizer, P. Lang, B. Heinz, M. Geilen, T. Brächer, P. Pirro, T. Meyer, and A. Conca, Determination of the spin Hall angle in single-crystalline Pt films from spin pumping experiments. *New J. Phys.* **20**, 053002 (2018).

[77] H. V. Gomonay, and V. M. Loktev, Spin transfer and current-induced switching in antiferromagnets. *Phys. Rev. B* **81**, 144427 (2010).

[78] H. Fujita, Field-free, spin-current control of magnetization in non-collinear chiral antiferromagnets. *Phys. Stat. Solidi RRL* **11**, 1600360 (2017).

[79] Y. Yamane, O. Gomonay, and J. Sinova, Dynamics of noncollinear antiferromagnetic textures driven by spin current injection. *Phys. Rev. B* **100**, 054415 (2019).

[80] M.-A. Leroy, A. M. Bataille, F. Bertran, P. Le Fèvre, A. Taleb-Ibrahimi, and S. Andrieu, Electronic structure of the Cr(001) surface and Cr/MgO interface, *Phys. Rev. B* **88**, 205134 (2013).

[81] M.-A. Leroy, A. M. Bataille, B Dkhil, F. Porcher, A. Barbier, V. L. R. Jacques, Y. Lu, C. Bellouard, T. Hauet, S. Ravy, J. H.-Martin, C. Gatel, K. Bouzehouane, A. Gukasov, S. Andrieu, and C. Tiusan, Tunnel-mediated coupling between antiferromagnetic thin films, *Phys. Rev. B* **90**, 035432 (2014).

[82] K. Momma and F. Izumi, VESTA: a three-dimensional visualization system for electronic and structural analysis. *J. Appl. Crystal.* **41**, 653 (2008).

[83] M. Kawamura, Fermisurfer: Fermi-surface viewer providing multiple representation schemes. *Comp. Phys. Commun.* **239**, 197 (2019).